DOI: 10.1534/genetics.107.075945

Bedraggled, a Putative Transporter, Influences the Tissue Polarity Complex During the R3/R4 Fate Decision in the Drosophila Eye

Amy S. Rawls, Sarah A. Schultz, Robi D. Mitra and Tanya Wolff[1]

Department of Genetics, Washington University School of Medicine, St. Louis, Missouri 63110

Manuscript received May 15, 2007
Accepted for publication June 24, 2007

ABSTRACT

The tissue polarity pathway is required for the establishment of epithelial polarity in a variety of vertebrate and invertebrate organs. Core tissue polarity proteins act in a dynamically regulated complex to direct the polarization of the Drosophila eye. We report the identification and characterization of *bedraggled* (*bdg*), a novel gene that regulates one output of the tissue polarity pathway—the establishment of the R3/R4 photoreceptor fates. *bdg* encodes a novel, putative transporter protein and interacts genetically with all of the core polarity genes to influence the specification of the R3 and R4 cell fates. Finally, *bdg* is required for both viability and the initial stages of imaginal disc development.

THE polarized orientation of cells within an epithelium, known as tissue or planar cell polarity, is essential to the development of functional organs. The core tissue polarity complex, composed of a conserved group of proteins, is required for patterning the polarized structures of both vertebrate and invertebrate epithelia. In mammals, for example, the uniform orientation of stereocilia (Dabdoub *et al.* 2003) and the polarized movements of cells in convergent extension (Myers *et al.* 2002) require the activity of this complex. The core tissue polarity proteins are also essential for patterning the polarized epithelia in Drosophila, including micro- and macrochaete, legs, and ommatidia. Tissue and/or cell function-specific modulators of the tissue polarity pathway control the differentiation of diverse epithelial organs.

The Drosophila eye is a planar epithelium consisting of ~800 unit eyes, called ommatidia. Eight of the 20 cells that compose each ommatidium are photoreceptors. The rhabdomeres, or light-sensitive organelles of the photoreceptors, are arranged in characteristic trapezoids that come in two chiral forms that show mirror-image symmetry across a midline, the equator (Figure 1A).

The Drosophila eye is precisely patterned during development. While thousands of genes cooperate to build an eye, a relatively small subset is required to polarize the epithelium (reviewed in Mlodzik 2005). Polarization of the eye is a multitiered process involving the cooperation of a long-range signal, the activity of the core tissue polarity complex, and Notch signaling. Long-range patterning systems initiate polarization in the eye with the establishment of an organizing center at the dorsoventral (D/V) boundary. Through the activity of a number of signaling molecules and pathways, dorsal and ventral fates are specified. The long-range polarity signal is transmitted by probably two parallel, nonredundant systems. The first of these systems is a set of gradients of at least three genes, *four-jointed* [a type II transmembrane protein (Zeidler *et al.* 1999; Strutt *et al.* 2004)], *fat*, and *dachsous* (atypical cadherins), which act via an unknown mechanism (Rawls *et al.* 2002; Yang *et al.* 2002). The second of these is the nonautonomous activity of *frizzled* (*fz*) and *strabismus* (*stbm*; also known as *Van Gogh*), two of the core tissue polarity genes. A complex consisting of the proteins encoded by *stbm* (Taylor *et al.* 1998; Wolff and Rubin 1998), *fz* (Vinson and Adler 1987; Vinson *et al.* 1989; Zheng *et al.* 1995), *flamingo* (*fmi*, also known as *starry night*) (Chae *et al.* 1999; Usui *et al.* 1999; Rawls and Wolff 2003), *dishevelled* (*dsh*) (Klingensmith *et al.* 1994; Theisen *et al.* 1994), *diego* (*dgo*) (Feiguin *et al.* 2001; Das *et al.* 2004), and *prickle* (*pk*) (Gubb *et al.* 1999; Tree *et al.* 2002), or the core tissue polarity complex, is a dynamically regulated signaling center that receives the global polarizing signal. Proper interpretation and execution of downstream events that establish the polarized epithelium requires that these proteins form asymmetric complexes in the photoreceptor (R) precursor cells, R3 and R4. The ultimate readout of the D/V signal is specification of the R3 and R4 cell fates via Notch signaling.

Two key events establish tissue polarity in the eye: specification of the R3 and R4 fates and the appropriate direction (and degree) of ommatidial rotation. In wild-type eyes, the polar, or more lateral, cell of the R3/R4 precursor pair adopts the R4 cell fate and the equatorial

[1]*Corresponding author:* Washington University School of Medicine, Campus Box 8232, 4566 Scott Ave., St. Louis, MO 63110.
E-mail: twolff@genetics.wustl.edu

cell, which is located closer to the midline, adopts the R3 cell fate. It is believed that fate specification precedes the second event, ommatidial rotation, in which precursors rotate 90° counterclockwise in the dorsal half of the eye and 90° clockwise in the ventral half. Furthermore, it is also thought that the R3 and R4 cells instruct the ommatidial precursor to rotate in the appropriate direction of rotation with respect to its dorsal or ventral location in the eye. In the discussion that follows, all definitions are based on the model that the direction of ommatidial rotation occurs with respect to the assigned R3 and R4 fates.

In the tissue polarity mutants, one or both of these two key events can be misprogrammed, leading to a distinct set of subclasses of mutant ommatidia, including inversions on the anterior/posterior (A/P) axis, the dorsal/ventral (D/V) axis, or both axes (AP/DV) (Wolff and Rubin 1998). In AP/DV inversions, the R3 and R4 fates are correctly specified, yet ommatidia rotate in the wrong direction with respect to those fates. In D/V inversions, the R3 and R4 fates are reversed, yet rotation still occurs in the correct direction with respect to the misspecified cells. A/P inversions arise when the R3 and R4 fates are reversed and the direction of rotation is inconsistent with respect to those fates [refer to Figure 1 for detailed description of subclasses (Wolff and Rubin 1998; Wolff *et al.* 2007)]. A fourth class of defects, known as "symmetric ommatidia," includes ommatidia with two R3 cells and no R4 cells (R3/R3) or two R4 cells and no R3 cells (R4/R4). The identities of cells comprising symmetric ommatidia were characterized in a landmark study by Cooper and Bray (1999), in which they correlated the molecular identity of R3 and R4 with the placement of rhabdomeres in an ommatidium. This study showed that symmetric R3/R3-type ommatidia are rectangular in shape whereas symmetric R4/R4-type ommatidia are square in shape.

The ommatidial defects described above, in combination with the fact that the mutant ommatidia often fail to rotate precisely 90°, cause a disruption of the normally smooth ommatidial lattice, giving the eye a "rough" texture. The ability to rapidly detect this phenotype enabled the identification of several of the core tissue polarity genes in large-scale loss-of-function screens. However, genes that contribute to the establishment of polarity, yet have either no or a very weak polarity phenotype, go undetected using this strategy. To circumvent this limitation in a search for new regulators of ommatidial polarity, we conducted a genetic modifier screen in a sensitized *stbm* background. Such modifier screens also provide an opportunity to identify genes that act redundantly with, downstream of, or in parallel to the core polarity complex to direct its output in a process-appropriate manner.

This screen identified *bdg*, a novel gene that is predicted to encode a transporter protein. *bdg* modifies the core tissue polarity genes to influence the R3 and R4 cell fates. An extensive genetic analysis demonstrates that *bdg* interacts with all of the core tissue polarity genes, but perhaps not with *Notch*, to influence the R3/R4 fate decision. While overexpression of *bdg* generates a moderate ommatidial polarity phenotype, polarity defects in *bdg* loss-of-function mutants are rare, suggesting functional redundancy with the core polarity complex. In addition, Bdg is required for viability and early imaginal disc development. Finally, *bdg* mutant escapers display several locomotor phenotypes typically seen in neurotransmission-deficient flies.

MATERIALS AND METHODS

Genetics and *P*-element screen: The Glass Multimer Reporter Enhancer-Promoter (GMREP) collection (generous gift from B. Hay) was used, which included bdg^{GMREP}, $CG8291^{KG07083}$, bdg^{36}, bdg^{90}, bdg^{164}, *sev-stbm*$^{14-1}$, *sev-stbm*$^{3-2}$, *sev-stbm*$^{3-4}$, *sev-stbm*$^{9-4}$, $stbm^{6cn}$, $stbm^{153}$, *sev-phyl*, *sev-fz*, *sev-dsh*, *sev-N*, *sev*-Gal4, UAS-bdg^{S1}, UAS-*fmi*, UAS-*dgo*, GMR-*phyl*, GMR-*Gal4*, L(2)*Pin/Kr*-GFP, CyO, pk^{pple}, dsh^{1}, fz^{19} (fz^{N21}), fz^{20}(fz^{J22}), dgo^{380}, fmi^{fz3}, $dIAP2^{GMREP}$, *P{ry*$^{+t7.2}$*=PZ}l(2)05248*^{05248} *cn1/CyO;* ry^{506}, *SpCyO*; Δ*2-3 Sb/TM6,* w^{1118}, and Canton-S.

For the dominant modifier screen, transgenic flies carrying two copies of the *sev-stbm* construct were crossed to ~1800 GMREP lines. The F_1 progeny were scored under the dissecting microscope for dominant modification of the *sev-stbm* rough eye phenotype; eyes from the 69 GMREP lines that showed an interaction were subsequently sectioned (as described by Wolff 2000a,b) and the phenotypes quantitated. Thirty-five enhancers and one suppressor of *sev-stbm* were confirmed as dominant modifiers of the *sev-stbm* phenotype (see Wolff *et al.* 2007 for details).

Phenotypic, statistic, and mosaic analyses: Adult eyes were fixed, embedded, and sectioned according to Wolff (2000). The number of ommatidia, *N*, and number of eyes (in parentheses) scored per genotype are included in detailed tables reporting phenotypic analyses. Because bdg^{90} is lethal, and since bdg^{90}, bdg^{36}, and bdg^{164} show consistent loss-of-function phenotypes and genetic interactions in the seven cases tested (supplemental Table 1 at http://www.genetics.org/supplemental/), bdg^{164} was used for all double-mutant analyses.

A *G*-test of independence was performed to determine if the *sev-stbm/P*-element lines displayed statistically significant differences in the classes of ommatidial defects compared to *sev-stbm*. The *G*-test is similar to the commonly used Pearson's chi-square test, but produces more accurate results for small sample sizes and makes possible a distinction between the component parts that comprise the overall change in phenotype. In other words, while two genotypes may have the same overall ommatidial phenotype, there can be dramatic differences in the subclasses of ommatidial phenotypes; the *G*-test of independence extracts these differences. Therefore, even though a standard deviation (SD) for a given interaction may be quite large, if the more diagnostic *P*-value is very small, the interaction is robust. For this test, between 411 and 2135 ommatidia from a minimum of five eyes of each modifier and background line were placed into the following categories: A/P inversions, D/V inversions, AP/DV inversions, R3/R3, R4/R4, fail to rotate (or missing photoreceptors), and normal. Two MATLAB scripts were written to calculate the *G* statistic (corrected by William's factor) as described in (Sokal 1995). These scripts can be downloaded from (http://www.genetics.wustl.edu/rmlab/gtest/).

bdg^{GMREP} overexpression clones were generated using standard FLP/FRT methods and mosaic R3/R4 pairs were scored for expression of the transgene. *bdg*^{90} clones were also generated using standard FLP/FRT methods using *ey*-FLP or using the FLP/FRT strategy in a *Minute* background.

***In situ* hybridization and Northern blot analysis:** For *in situ* hybridization studies of candidate genes, third instar eye discs were dissected and processed as described (Wolff 2000a,b). Antisense and sense DIG-labeled RNA probes of the following candidate genes were generated from EST clones (Research Genetics, Birmingham, AL): *CG8291* (*bdg*) (clone SD06837), *CG8297* (clone SD23639), and *MLF* (clone SD02769), according to manufacturer's protocol (Roche Molecular Biochemicals). *In situ* hybridization was carried out according to established protocol, using 1 μg of DIG-labeled RNA probe (Wolff 2000a,b). For Northern blot analysis of *bdg*, 30 third instar larvae were homogenized in Trizol reagent, and total RNA was extracted according to the manufacturer's protocol (GIBCO, Grand Island, NY). Twenty-five nanograms of RNA were analyzed according to standard protocol (Sambrook *et al.* 1989) using ^{32}P-labeled probe ($\sim 2 \times 10^7$ CPM) generated from cDNA clone SD06837.

Immunohistology: Third larval instar eye discs were dissected and processed (Wolff 2000a,b). Primary antibody incubations were conducted at 4° overnight, at the following concentrations: α-dIAP2 1:50 (Huh *et al.* 2007), α-Stbm 1:500, α-Fmi 1:10 (Usui *et al.* 1999; generous gift from T. Uemura), α-Arm 1:10 (Developmental Studies Hybridoma Bank, University of Iowa), and α-GABA 1:100 (gift of R. Wong). Secondary antibodies conjugated to Alexafluor fluorescent dyes were used at 1:200 according to the manufacturer's protocol (Molecular Probes, Eugene, OR).

Phylogenetic analysis of Bdg: Nine proteins most similar to the Bdg amino acid sequence were determined using NCBI-BlastP (Altschul and Lipman 1990). The Drosophila serotonin transporter (*Ser T*) was also included. A multiple sequence alignment was generated using Clustal X (Thompson *et al.* 1997). The neighbor-joining tree was generated from 1000 iterations of the *u*nweighted *p*air *g*roup *m*ethod with *a*rithmetic means (UPGMA).

***P*-element excision screen for *bdg* deletion alleles:** *bdg*^{GMREP} females were crossed to *Sp/CyO*; *Δ2-3 Sb/TM6* males and 20,000 F_2 genomes were scored for loss of the w^+ transgene. Individuals with potential excisions were subjected to a PCR-based analysis of the genomic region. Three *bdg* alleles, *bdg*^{36}, *bdg*^{90}, and *bdg*^{164}, were identified using this approach, and PCR was used to map minimal deletions in these alleles (see supplemental methods at http://www.genetics.org/supplemental/). The *bdg* locus encodes three transcripts, each of which produces an identical 1331-amino-acid protein (FlyBase, Indiana University; Figure 2A) due to the use of a shared translational start in exon 2. The deletions in *bdg*^{36} and *bdg*^{164} alleles are contained within the large intron, leaving exons 1 and 2 intact. Exon 2 is deleted in *bdg*^{90}, the predicted null allele.

Generation of UAS-*bdg* transgenic flies: The *CG8291-RB* (*bdg*) transcript was amplified by PCR from the full-length cDNA clone, SD06851 (Research Genetics), using 5′ GAC AAATCAGCTGCGACATC and 3′ AAGCAAGCGGATATGTG GAT primers. The 5′ and 3′ primer included *Bgl*II and *Not*I sites, respectively, and the PCR product was directionally cloned into pUASt. Automated sequencing (Big Dye V3 chemistry; ABI Prism 3100 sequencer, Applied Biosystems, Foster City, CA) confirmed that the construct represented the full-length wild-type *bdg* cDNA. pUASt-*bdg* DNA was injected into nondechorionated embryos within 1 hr after egg laying at 200 ng/λ with 50 ng/λ of s129A helper DNA (Beall *et al.* 2002), according to established protocol (Rubin and Spradling 1982). Six hundred embryos were injected. Ninety surviving founders were backcrossed to w^{1118} and F_1 progeny were screened for the w^+ transgene. Six transformants were isolated, and UAS-*bdg*^{S1} was used for overexpression and rescue experiments.

RESULTS

***bdg*^{GMREP} is a dominant suppressor of *sev-stbm*:** *bedraggled* (*bdg*), a novel gene that encodes a putative transporter protein, was identified in an F_1 dominant modifier screen as a suppressor of the tissue polarity gene *stbm*, under the control of the *sevenless* (*sev*) promoter. This screen was carried out in a sensitized genetic background in which the *sev* promoter was used to drive high levels of *stbm* expression (*sev-stbm*) in photoreceptors R3, R4, R7, and the nonneuronal cone cells. Misexpression of *stbm* in this subset of cells results in a mild ommatidial polarity phenotype: flies carrying one copy of the *sev-stbm* transgene inserted on the second chromosome (*sev-stbm*$^{14\text{-}1}$) exhibit polarity defects in 15.4% of ommatidia (Figure 1C) (Rawls and Wolff 2003). Since this degree of disruption, as well as enhancement and suppression of this phenotype, can be readily detected at the dissecting microscope level, *sev-stbm*$^{14\text{-}1}$ was used as the genetic background for the screen. Briefly, flies carrying two copies of the *sev-stbm*$^{14\text{-}1}$ insertion were independently crossed to 1800 uncharacterized *P*-element lines [GMREP collection (Hay *et al.* 1997); generous gift of B. Hay] and the F_1 progeny were examined for an enhanced or suppressed degree of eye roughness. Thirty-five GMREP lines were found to enhance (Wolff *et al.* 2007) and one was found to suppress the *sev-stbm* mild rough-eye phenotype (Figure 1, B and D). Notably, it is rare to identify suppressors of tissue polarity genes—*bdg* represents one of only three suppressors of *sev-stbm* that have been identified in our lab in ~4000 lines screened. Characterization of the suppressor identified in this screen, which we have named *bedraggled* for its appearance after getting stuck in the food due to defects in motor coordination, is described here.

One copy of the *bdg P*-element line, *bdg*^{GMREP}, suppresses the *sev-stbm*$^{14\text{-}1}$/+ phenotype from one in which 15.4% of ommatidia have defects in polarity to one in which only 3.4% are mutant (Figure 1, B and D; Table 1); note that the *P*-value, not the SD, is the indicator of significance of the interaction, as discussed in materials and methods). This genetic interaction was reproducible in three additional *sev-stbm* lines tested: the *sev-stbm*$^{3\text{-}2}$ phenotype is suppressed from 8.8 to 1.4%, *sev-stbm*$^{3\text{-}4}$ from 9.4 to 1.7%, and *sev-stbm*$^{9\text{-}4}$ from 21.0 to 0.9%. The genetic interaction between *sev-stbm* and *bdg*^{GMREP} is specific to the function of these genes and is not due to a nonspecific effect on the promoters, as *bdg*^{GMREP} does not dominantly modify the *sev-phyllopod (phyl)* phenotype nor does *sev-stbm* modify the GMR-*phyl* phenotype (data

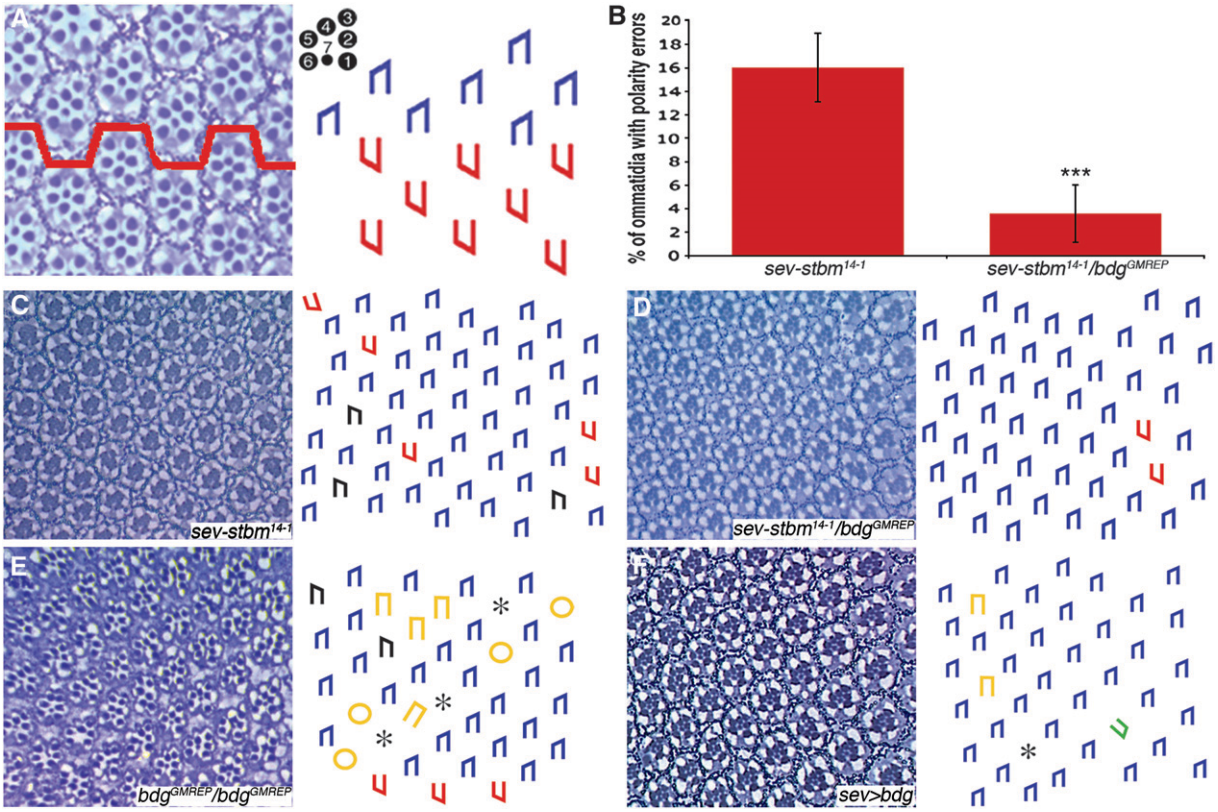

FIGURE 1.—The overexpression of *bdg* suppresses *sev-stbm* and generates an ommatidial polarity phenotype. Tangential sections through adult eyes (left) and corresponding schematics (right) are shown. In a wild-type eye (A), chiral ommatidia are arranged with respect to the dorsal/ventral midline of mirror symmetry known as the equator (red line), such that those in the dorsal (blue trapezoids) and ventral (red trapezoids) hemispheres orient toward the dorsal and ventral poles, respectively. (B–D) bdg^{GMREP} suppresses the mild *sev-stbm* phenotype from one in which ~15% of ommatidia have polarity errors (B and C) to one in which only ~3% have defects (B and D). Error bars represent standard deviation (SD) and triple asterisks indicate $P < 10^{-9}$. Many of the results that follow are displayed in both histogram and table format. The histograms indicate SD between individuals, whereas the *P*-values in the tables provide a more stringent evaluation of the data, as the $R \times C$ test of independence accounts for each type of polarity error as an independent event (see MATERIALS AND METHODS). It is therefore the *P*-value that indicates the robustness of the interaction. (E) Flies with two copies of bdg^{GMREP} have an ommatidial phenotype, and (F) *sev>bdg* transgenic animals have a similar, but less penetrant, phenotype. Green trapezoid: AP/DV inversion. Yellow shapes denote symmetrical ommatidia (rectangles, R3/R3; circles, R4/R4) and asterisks indicate missing photoreceptors.

not shown). To confirm the role for *bdg* in the tissue polarity signaling pathway suggested by these overexpression data, we carried out extensive loss-of-function genetic analyses, as described below.

bdg^{GMREP} is an overexpression line of annotated gene *CG8291*: The *P*-element transposon in bdg^{GMREP} contains the *g*lass *m*ultimer *r*eporter (GMR) with its endogenous *e*nhancer-*p*romoter element (EP). GMR is an eye-specific driver in cells posterior to the morphogenetic furrow of the eye imaginal disc (HAY *et al.* 1997). The EP element can exert its effect on genes that lie within 10 kb upstream or downstream of the *P* element (HAY *et al.* 1997). Consequently, phenotypes in the GMREP, *sev-stbm* lines can be the result of (1) disruption of the gene into which the *P* element inserts or (2) overexpression of a gene that lies within 10 kb of the insertion site.

As a first step in identifying the gene responsible for the interaction with *sev-stbm* and characterizing the nature of the effect [*i.e.*, loss of function due to the disruption of a gene *vs.* mis- or overexpression of a nearby gene(s)], we used plasmid rescue to isolate the genomic DNA surrounding the *GMREP* insertion and subsequently cloned and sequenced this DNA. The *P* element is inserted at cytological position 52D2 and disrupts the 5′ region of annotated gene *CG8291* (Figure 2A). Three additional genes, *Drosophila inhibitor of apoptosis 2* (*dIAP2*), *myologenous leukemia factor* (*MLF*), and annotated gene *CG8297*, lie within 20 kb (+10 to −10 kb) of the insertion site and were therefore also considered candidate interactors. However, genetic interaction data (not shown) and *in situ* hybridization analysis eliminated these three genes as candidates. *In situ* hybridization of wild-type and bdg^{GMREP} third larval instar eye imaginal discs revealed that *CG8297* and *MLF* transcripts are expressed at wild-type levels in bdg^{GMREP} discs (data not shown), whereas *CG8291* is overexpressed in bdg^{GMREP} discs (Figure 2B). dIAP2 protein is also present at wild-type levels in bdg^{GMREP} discs (data not

TABLE 1

***bdg* interacts with the core tissue polarity genes in overexpression and loss-of-function analyses**

Genotype	A/P (%)	D/V (%)	AP/DV (%)	R3/R3 (%)	R4/R4 (%)	FTR (%)	Total errors (%)	*N*
sev-stbm$^{14\text{-}1}$/+	5.5	6.3	0.4	1.2	2.2	0	15.5	2135 (20)
*sev-stbm$^{14\text{-}1}$/bdg^{GMREP}***	1.2	1.5	0.2	0.3	0.3	0	3.4	1892 (20)
*sev-stbm$^{14\text{-}1}$/bdg^{164}***	7.0	11.5	3.1	0.7	2.6	0.7	25.5	1537 (13)
stbm^{6cn}/stbm^{6cn}	10.6	21.9	3.6	4.3	1.6	2.3	44.3	1328 (12)
*stbm^{6cn}, bdg^{GMREP}/stbm^{6cn}****	12.6	27.7	2.3	1.0	1.3	0	45.0	1240 (16)
*stbm^{6cn}, bdg^{164}/stbm^{6cn}, bdg^{164}****	9.7	26.3	4.5	13.8	4.9	1.7	61.1	1488 (15)
stbm^{153}/stbm^{153}	11.3	18.6	3.0	0.4	1.4	1.5	36.2	1049 (11)
*stbm^{153}, bdg^{164}/stbm^{153}, bdg^{164}****	8.8	12.9	3.0	23.2	4.4	1.8	53.9	799 (8)
sev-dsh/+	3.4	2.3	2.4	1.9	0.6	0	10.5	1006 (9)
*sev-dsh/bdg^{GMREP}**	5.0	3.8	2.6	3.7	1.6	0	16.7	1336 (11)
sev-dsh/bdg^{164}	3.0	2.6	3.5	1.0	1.0	0	11.1	800 (7)
dsh^{1}/Y	9.4	6.3	4.9	2.2	0.6	1.3	24.7	956 (9)
*dsh^{1}/Y; bdg^{GMREP}/+****	14.3	11.8	6.3	3.6	5.2	1.1	42.4	441 (5)
*dsh^{1}/Y; bdg^{164}/+****	8.4	7.0	4.9	4.4	6.4	0.4	31.6	699 (6)
*dsh^{1}/Y; bdg^{164}/bdg^{164}****	12.9	10.3	5.4	25.6	7.0	0.8	61.9	1268 (8)
pk^{sple}/pk^{sple}	1.1	41.5	1.9	1.6	0.8	0	46.9	744 (7)
pk^{sple}, bdg^{GMREP}/pk^{sple}	2.1	39.2	1.2	0.5	0.9	0	43.9	864 (10)
*pk^{sple}, bdg^{164}/pk^{sple}, bdg^{164}****	2.7	31.1	1.1	9.2	3.4	0.1	47.6	818 (9)
sev-fmi/Y	9.7	31.9	2.2	0.7	0.4	0.6	45.6	1253 (10)
*sev-fmi/Y; bdg^{GMREP}/+**	13.3	27.3	2.8	0.8	1.1	0.1	45.5	714 (6)
*sev-fmi/Y; bdg^{164}/+**	7.8	24.9	2.5	1.9	2.3	0.2	39.6	606 (6)
fmi^{frz3}/fmi^{frz3}	9.6	5.4	2.7	3.6	1.2	0.7	23.2	1073 (12)
*fmi^{frz3}, bdg^{GMREP}/fmi^{frz3}****	13.5	23.7	4.2	2.0	0.6	0.9	44.9	801 (9)
*fmi^{frz3}, bdg^{164}/fmi^{frz3}, bdg^{164}****	6.1	5.2	3.6	12.5	8.7	0	35.9	473 (6)
sev::dgo2C/+	19.6	0.8	1.4	2.8	0.4	3.0	28.1	855 (9)
*sev::dgo2C; bdg^{GMREP}/+****	31.5	2.4	0.8	6.7	4.4	1.5	47.3	723 (8)
*sev::dgo2C; bdg^{164}/+****	18.8	1.0	0.4	10.4	3.0	3.7	37.3	789 (8)
dgo^{380}/dgo^{380}	3.6	1.4	0.5	13.2	14.1	0.6	33.5	937 (9)
*dgo^{380}, bdg^{GMREP}/dgo^{380}****	6.3	3.2	1.1	4.3	5.0	0.1	20.0	916 (10)
*dgo^{380}, bdg^{164}/dgo^{380}****	2.2	0.9	0.9	8.6	5.4	0.2	18.1	778 (9)
dgo^{380}, bdg^{164}/dgo^{380}, bdg^{164}				Lethal				
sev-fz/+	11.2	6.3	6.1	29.9	13.2	0	66.7	839 (9)
*bdg^{GMREP}/+; sev-fz/+***	17.1	8.1	4.6	18.8	14.6	0	63.1	919 (7)
bdg^{164}/+; sev-fz	10.0	7.1	4.4	32.7	12.4	0	66.6	661 (7)
fz^{N21}/fz^{J22}	5.6	4.9	3.1	0.1	0.3	1.5	15.6	744 (8)
*bdg^{GMREP}/+; fz^{N21}/fz^{J22}**	6.3	6.8	5.5	0.2	0.7	0.2	19.7	867 (9)
bdg^{164}/+; fz^{N21}/fz^{J22}	5.2	4.0	1.6	0.4	0.5	0.2	11.9	965 (10)
*bdg^{164}/bdg^{164}; fz^{N21}/fz^{J22}****	7.8	7.3	3.5	5.8	1.6	0.3	26.4	1180 (7)

FTR, failure to rotate; *N*, number of ommatidia scored (eyes scored). Statistical significance is measured by a *G*-test of independence. The underlined genotype is the reference in each data set. **P*-value $<10^{-3}$; ***P*-value $<10^{-6}$; ****P*-value $<10^{-9}$.

shown). Finally, Northern blot analysis revealed that the *CG8291* transcript is more abundant in total RNA isolated from *bdg^{GMREP}* larvae than in total RNA isolated from wild-type larvae (supplemental Figure 1 at http://www.genetics.org/supplemental/).

Additional evidence that CG8291 is the gene responsible for the *bdg^{GMREP}* phenotypes comes from the analysis of a second *P*-element insertion in *CG8291*, *CG8291^{KG07083}* (BDGP). This experimentally uncharacterized *P* element also maps to the 5′ region of *CG8291* (Figure 2A) and is predicted to disrupt the transcriptional activity of CG8291. *CG8291^{KG07083}* dominantly enhances the phenotype: the *sev-stbm* phenotype is enhanced approximately twofold, from 15.4% ommatidial errors to 30% ommatidial errors (supplemental Figure 2 at http://www.genetics.org/supplemental/). (A further characterization of this interaction was conducted using confirmed loss-of-function alleles of *bdg*, generated by imprecise excision, as discussed below.)

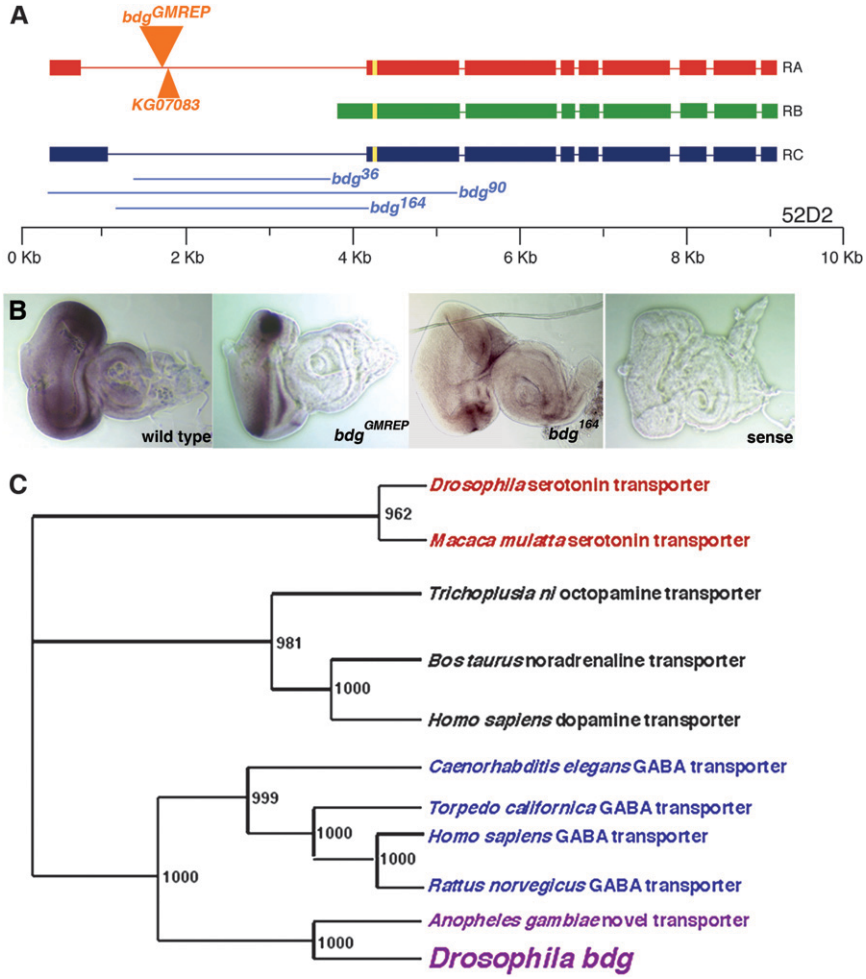

FIGURE 2.—Annotated gene *CG8291* is *bdg* and encodes a novel transporter protein. (A) The *CG8291* locus at chromosomal position 52D2 generates three mRNA transcripts (RA, RB, and RC), each of which encodes the same protein due to use of a common translation start site (yellow boxes). The bdg^{GMREP} and *KG07083 P*-element insertions map to the large intron (orange triangles). The regions deleted in each of the *bdg* loss-of-function alleles are illustrated as blue lines for each allele. (B) *In situ* hybridization of *CG8291*-RB probe in third instar eye discs suggests that *bdg* is *CG8291*. (C) Phylogenetic analysis of *bdg* reveals that it is a novel member of the sodium-dependent neurotransmitter transporter family, most closely related to the GABA transporters.

Finally, the *bdg* cDNA was used to generate UAS-*bdg* transgenic animals. Standard rescue experiments were not possible, as overexpression of *bdg* throughout the body, using either actin- or hs-Gal4, is lethal. As an alternative, we demonstrated that *bdg* driven by GMR recapitulates the bdg^{GMREP} homozygous phenotype (see below; Table 2). Additionally, UAS-*bdg*::sev-*Gal4* transgenic flies reproduce, albeit weakly, the bdg^{GMREP} eye phenotype (Figure 1F; Table 2). Together, these molecular and genetic data demonstrate that *CG8291* is *bdg*.

Bdg is a putative transporter protein: Bdg is encoded by a novel gene and is annotated as a neurotransmitter:sodium symporter (Berkeley Drosophila Genome

TABLE 2

All core tissue polarity genes, except *fz*, dominantly suppress bdg^{GMREP} overexpression phenotype

Genotype	A/P (%)	D/V (%)	AP/DV (%)	R3/R3 (%)	R4/R4 (%)	Missing R (%)	Total errors (%)	*N*
bdg^{GMREP}/bdg^{GMREP}	1.6	0.4	0.2	6.8	3.0	8.1	20.1	894 (10)
$stbm^{6cn}$, bdg^{GMREP}/bdg^{GMREP}***	0	0.1	0.1	0.7	0.2	2.0	3.1	912 (8)
$dsh^{1}/+$; bdg^{GMREP}/bdg^{GMREP}***	0.4	0.1	0	0.1	0.3	0.3	1.2	730 (9)
pk^{sple}, bdg^{GMREP}/bdg^{GMREP}***	0.4	1.6	0	2.8	1.9	1.9	8.6	573 (5)
fmi^{frz3}, bdg^{GMREP}/bdg^{GMREP}***	0.4	0.6	0	0.6	1.0	0.8	3.4	495 (6)
dgo^{380}, bdg^{GMREP}/bdg^{GMREP}***	0.2	0.7	0.2	1.1	0.7	1.8	4.6	565 (6)
bdg^{GMREP}/bdg^{GMREP}; $fz^{J22}/+$	1.5	0.5	0	2.9	4.4	7.1	16.3	411 (5)
GMR-*Gal4RC*/+;UAS-*bdg*/UAS-*bdg*	1.1	0.1	0.1	5.2	2.0	5.3	13.9	699 (13)
sev-Gal4/*sev*-Gal4;UAS-*bdg*/UAS-*bdg*	0.1	0	0.3	1.2	0	0.4	2.0	1852 (12)

N, number of ommatidia scored (eyes scored). Statistical significance was measured by a *G*-test of independence. The underlined genotype is the reference for this data set. ***P-value $<10^{-9}$.

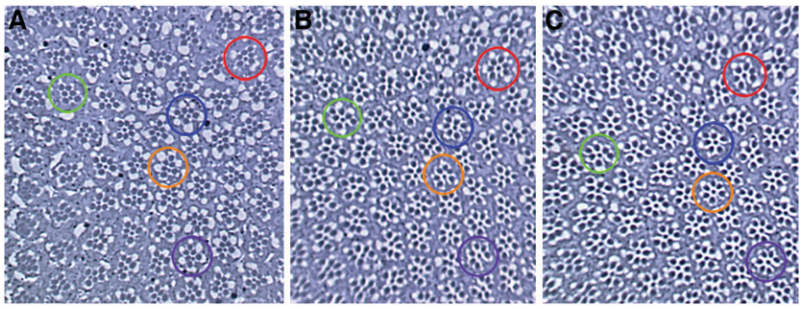

Figure 3.—Trapezoid morphology of mutant ommatidia can change between focal planes. Thirty-nine percent of mutant ommatidia in $dsh^{1}/dsh^{1};bdg^{GMREP}/bdg^{GMREP}$ eyes "morph" throughout the apical portion of the eye. A subset of morphed ommatidia is highlighted; each color represents a single ommatidium at three distinct focal planes that bisect the eye at the level of the R7 rhabdomere. For example, the ommatidium circled in orange appears to have two R3 cells in the most apical plane (A), wild-type morphology in an intermediate plane (B), and two R4 cells in the most basal plane (C).

Project, BDGP), a protein that uses energy from the cotransport of Na^+ and Cl^- to transport a neurotransmitter against its concentration gradient. Our phylogenetic analysis indicates that Bdg is most closely related to the sodium-dependent GABA transporter family (Figure 2C). A hydrophobicity analysis of Bdg predicts that it contains 11 or 12 transmembrane domains [derived using TMHMM, a transmembrane helix prediction program (Sonnhammer *et al.* 1998)], in agreement with the BDGP annotation of CG8291 as an integral membrane protein. This finding is consistent with the idea that Bdg is a transporter with a hydrophobic core that constructs a channel for sodium-dependent transport.

To test the possibility that Bdg is transporting GABA, we (1) assayed GABA expression in the developing eye and (2) studied the effect of inhibition of GABA transport. While we did detect high levels of GABA in the larval brain, GABA was undetectable in the third larval eye imaginal disc (supplemental Figure 3 at http://www.genetics.org/supplemental/). Furthermore, nipecotic acid, a pharmacological inhibitor of GABA transport, did not result in an ommatidial polarity phenotype nor did it modify the *sev-stbm* phenotype (data not shown; methods according to Leal and Neckameyer 2002). These data suggest that Bdg does not transport GABA in the developing eye.

The only convincing non-drosophilid homolog of Bdg is a novel transporter in the genome of the mosquito, *Anopheles gambiae* (gene identifier: *agCG55776*). While there is no functional or structural information available for this homolog, Bdg and agCG55776 may represent a novel insect-specific transporter. Expression studies of *CG8291* in the embryo indicate that *bdg* transcript is abundant in the developing CNS, a pattern consistent with its predicted role as a neurotransmitter transporter (Kearney *et al.* 2004). The hydrophobicity data, together with our phylogenetic analysis and the published embryonic expression study, make a correlative argument that Bdg functions in the transport of a small molecule (on the order of 100–200 Da); this small molecule could be a neurotransmitter, an ion, or an amino acid. An alternative possibility is that *bdg* encodes a signaling molecule.

Trapezoid morphing: trapezoid shape can be plane dependent: Tomlinson and Struhl (1999) noted that the rhabdomeres of mutant ommatidia can assume different arrangements relative to one another at different depths within the retina. For example, an ommatidium that appears squat in shape and is characteristic of symmetric R4/R4-type ommatidia (Fanto *et al.* 1998; Cooper and Bray 1999) can look distinctly different at a more apical or basal plane. Due to the nature of the phenotypes explored in our studies, it was necessary to extend the original observation by Tomlinson and Struhl to include wild type, several mutants, and a sufficiently large sample size to establish whether their observation was a rare or a common phenomenon and if this phenomenon occurs in wild type or if it is unique to ommatidia with certain phenotypes.

Ommatidia were analyzed in at least three focal planes at the level of the R7 rhabdomere to exclude differences in rhabdomeral arrangement that occur at the R8 level (Figure 3). Our analysis indicates that "trapezoid morphing" does not occur in wild type (zero incidents in ~1200 ommatidia scored from 12 eyes), but does occur in assorted mutants and therefore is not unique to *bdg*. We analyzed eyes from *dsh;bdg* and *bdg;fz* double mutants, as well as from a random GMREP line that exhibits polarity defects, and found that a significant percentage of ommatidia undergo trapezoid morphing: 39% of mutant ommatidia morph in *dsh;bdg* double-mutant eyes (320 ommatidia analyzed in 13 eyes) (Figure 3, see legend for details). Some aberrant ommatidia were likely missed in the quantification of the *bdg/* tissue polarity genetic interactions due to trapezoid morphing. However, since these mutant ommatidia would be missed with equal probability in all genotypes, the data reported in Table 1 accurately reflect the genetic interactions.

Overexpression of *bdg* generates an eye phenotype: Eyes from bdg^{GMREP} flies exhibit a tissue polarity phenotype. Flies carrying one copy of the bdg^{GMREP} transgene are wild type (data not shown), but in the presence of two copies, 12% of ommatidia have defects in polarity. An additional 8% are missing photoreceptors, so the polarity of these ommatidia could not be assayed (Figure 1E; Table 2). Of these polarity defects, 82%—a strikingly large proportion—are due to problems in specification of the R3 and R4 cell fates (Table 2), as the trapezoids are symmetric in shape. Fifty-seven percent of these ommatidia have a characteristic "rectangular trapezoid" shape, a shape indicative of two R3 cells and

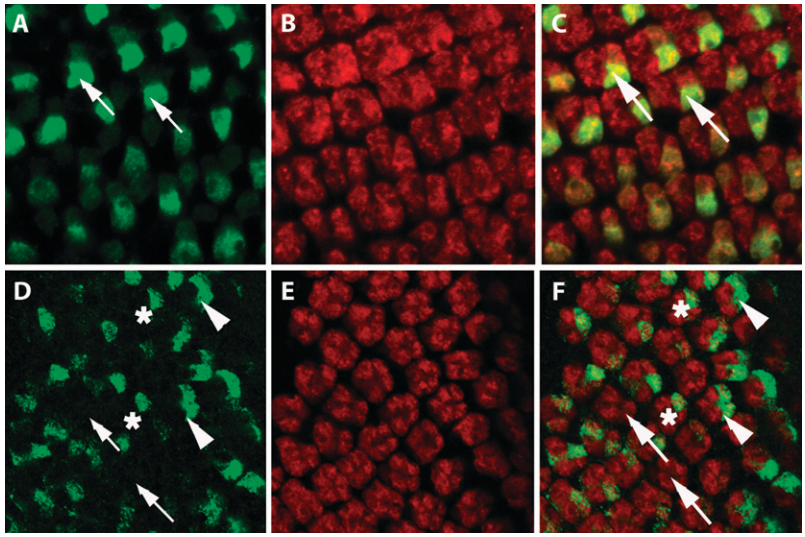

FIGURE 4.—An R4-specific marker reveals that the R3 and R4 cells are incorrectly specified in *dsh, bdgGMREP* imaginal discs. (A–C) *m*δ 0.5 in a wild-type background and (D–F) *dsh*^{1}*/Y; bdg*^{GMREP}*/+; m*δ *0.5/+* third instar eye imaginal discs stained with α-β-gal to identify the R4-specific Notch target, *m*δ 0.5 (green; A and D), and a-Elav (red; B and E), a pan-neuronal marker used here to label photoreceptor nuclei. Overlays are shown in C and F. In wild-type discs, one cell per cluster is identified as R4 by *m*δ 0.5 (A and C, arrows), whereas in the mutant tissue, ommatidial precursors exhibit a variety of defects, including: two *m*δ 0.5-positive cells, indicative of two R4 cells (D and F, arrowheads); zero *m*δ 0.5-positive cells, indicative of two R3 cells (D and F, arrows); or one *m*δ 0.5-cell, indicating a wild-type complement of cells (one R3 and one R4; D and F, asterisks). These results are consistent with the assignments of symmetric R3/R3- and R4/R4-type ommatidia in adult sections. Anterior is to the right.

no R4 cells (symmetric R3/R3-type ommatidia) and 25% of ommatidia are "squat" in shape, likely a consequence of a failure to specify the R3 fate, giving rise to ommatidia that have two R4 cells and no R3 cells (symmetric R4/R4-type ommatidia) (Figure 1E). (An analysis of the molecular identity of these cells was reserved for the loss-of-function tissue polarity studies described below.)

Notably, despite the significant number of symmetric ommatidia in *bdg*^{GMREP} flies, the external surface of the eye remains smooth. In contrast with tissue polarity mutants, the lattice is perfectly maintained due to wild-type rotation of these mutant ommatidia.

***bdg*^{GMREP} modifies the ommatidial polarity phenotypes of core tissue polarity genes:** A detailed description of the interactions discussed in this and the following sections is found in Table 1. Note that statistical significance indicated may be due to modification of specific subclasses rather than the overall phenotype, as explained in MATERIALS AND METHODS.

bdg^{GMREP} significantly modifies the eye polarity phenotypes of *stbm, dsh, fmi, dgo,* and *fz,* but not of *pk.* While *stbm, dsh, fmi,* and *fz* are all enhanced by *bdg*^{GMREP}, *dgo* is the only core tissue polarity gene that is suppressed by *bdg*^{GMREP}. The R3 and R4 fate decisions are predominantly modified in these interactions, with the exception of the *bdg, fz* interaction. This initial genetic characterization suggests that *bdg* (i) is important for the specification of a single R3 cell and a single R4 cell, (ii) can uniquely modify members of the polarity complex, and (iii) interacts with the core polarity genes (with the possible exception of *fz*) to influence the R3 and R4 fates.

R3 and R4 cell identities in the analyses described above were characterized on the basis of ommatidial morphology, as defined by COOPER and BRAY (1999). We confirmed these assignments of cell fate using the R4-specific marker *m*δ-*lacZ* (COOPER and BRAY 1999). Ommatidial precursors from *dsh*/Y; *bdg*^{GMREP}/+; *m*δ-*lacZ*/+ exhibit either symmetric staining in the R3 and R4 precursors, including clusters with two or zero lacZ-positive cells, or the wild-type asymmetry (Figure 4). These results are consistent with the assignments made in adult eyes and thereby confirm our interpretation that Bdg is important for the R3/R4 cell fate decision. Since the adult phenotype (scored on the basis of morphology) is consistent with the larval phenotype (scored on the basis of molecular markers), all subsequent analyses were conducted in the adult to enable the sampling of a sufficient number of ommatidia required for our rigorous statistical analysis.

***bdg* is required broadly for organismal viability, imaginal disc development, and motor coordination:** Multiple loss-of-function alleles of *bdg* were generated by imprecise excision of the *bdg*^{GMREP} transgene. Three of these alleles were characterized in detail at the molecular, phenotypic, and genetic levels. Two of these three alleles, *bdg*^{36} and *bdg*^{164}, are likely to be hypomorphic alleles while the third, *bdg*^{90}, is likely null, based on molecular and genetic analyses. PCR-based analysis indicates that exon 2, which encodes the translation start site (Figure 2A), is deleted in *bdg*^{90} mutants. *In situ* hybridization reveals that larvae homozygous for the *bdg*^{36} allele appear to have wild-type to slightly reduced levels of *bdg* transcript (data not shown) and *bdg*^{164} larvae have reduced transcript levels (Figure 2B). The *bdg* transcript in *bdg*^{90} larvae cannot be accurately measured due to their severely reduced eye imaginal discs (see below).

Bdg is required for viability: each of the three alleles described above is homozygous lethal, although occasional *bdg*^{36} and *bdg*^{164} escapers survive to eclosion. Bdg plays a role in early morphogenesis of the imaginal discs, as these structures are dramatically diminished in size in third instar larvae homozygous for *bdg*^{90}; notably, overall larval size is normal (see Figure 5 for eye and antennal discs). *bdg*^{36} and *bdg*^{164} escapers do not exhibit abnormalities in thorax or wing hair polarity (data not shown). However, on the basis of the eye phenotype

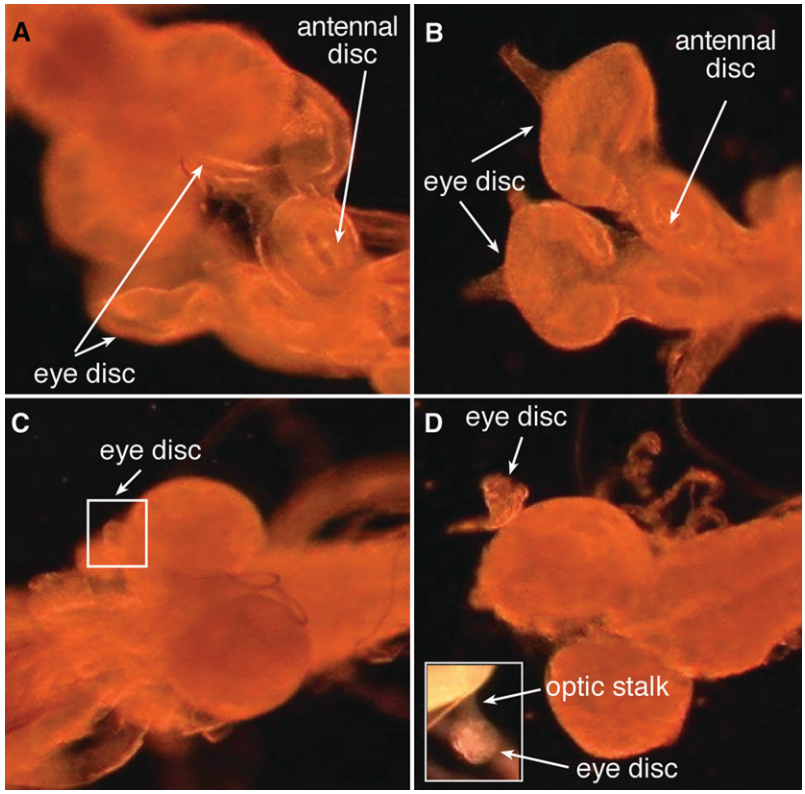

FIGURE 5.—Eye and antennal imaginal discs are significantly reduced in *bdg* null larvae. Wild-type (A and B) and bdg^{90} (C and D) eye-antennal imaginal discs are shown. Eye-antennal imaginal discs were removed from the brain (B) to better illustrate the size of wild-type discs. *bdg* null discs are ill-defined masses of tissue (C and D). A *bdg* eye disc attached to the brain via the optic stalk can be distinguished in D.

(described below), we speculate that if there are phenotypes in these tissues, they would be of such low penetrance that it would not be feasible to unambiguously define them as genetic defects (for example, an occasional misoriented hair could be due to mechanical disruption), so we cannot determine if *bdg* plays a role in these aspects of development.

bdg also plays critical roles in later developmental events in the eye, and at least one of these roles is likely to be redundant with other genes (perhaps the core tissue polarity genes). Analysis of bdg^{164} escaper eyes and bdg^{90} mutant clones revealed that while the vast majority of *bdg* mutant ommatidia are wild type, two phenotypes do occur: some ommatidia are missing photoreceptors and a small fraction show defects in R3/R4 fate specification (Figure 6, A–E; both phenotypes are consistent with the overexpression line, bdg^{GMREP}); of >2200 bdg^{90} ommatidia surveyed, only 10 symmetric ommatidia were identified in *bdg* null clones. The low frequency of symmetric ommatidia in null clones raises the possibility that *bdg* acts redundantly with other genes involved in R3/R4 fate specification.

Finally, *bdg* is essential for motor coordination. bdg^{36} and bdg^{164} escapers are grossly uncoordinated—upon eclosion, they immediately fall into the food and die (hence the name, *bedraggled*). If these flies are retrieved before getting stuck in the food, they are unable to fly, they exhibit a severely delayed righting reflex, and although escapers appear to walk normally, they have impaired climbing behavior. The behavioral defects we observe in *bdg* mutants are similar to those reported for some flies with defective neurotransmission (ARREDONDO *et al.* 1998; LEAL and NECKAMEYER 2002; NICHOLS *et al.* 2002; GODENSCHWEGE *et al.* 2004), raising the possibility that the *bdg* phenotype arises as a consequence of a deficiency in neurotransmitter transport.

***bdg* loss-of-function alleles interact with all core tissue polarity genes:** Loss-of-function *bdg* also interacts with *sev-stbm*: bdg^{164} dominantly enhances the *sev-stbm* phenotype from one in which 15.4% of ommatidia have polarity errors to one in which 25.5% have defects. This enhancement results primarily from an increase in D/V inversions, which have their basis in an R3/R4 fate reversal (Figure 7, A, B, and G; Table 1). Additionally, bdg^{164} dominantly suppresses *sev>fmi* (45.6–39.6%), again due almost entirely to suppression of D/V inversions (Figure 7, C, D, and G; Table 1). *sev>dgo* is also enhanced by bdg^{164} (28.1–37.3%), but this enhancement results entirely from an increase of symmetric R3/R3- and R4/R4-type ommatidia (Figure 7, E–G; Table 1). Interestingly, loss of *bdg* function does not modify the *sev-dsh* or *sev-fz* phenotypes (Table 1). bdg^{164} was used in all loss-of-function analyses; bdg^{164} and bdg^{90} show consistent genetic interactions (see MATERIALS AND METHODS and supplemental Table 1 at http://www.genetics.org/supplemental/).

None of the *bdg* alleles tested—bdg^{GMREP}, bdg^{90}, or bdg^{164}—exhibited genetic interactions with *sev-Notch* (supplemental Figure 4 at http://www.genetics.org/supplemental/, see legend for details). Even though all of the core tissue polarity genes interacted with *bdg* in at least one of these genetic assays, we cannot rule out the possibility that *Notch* interacts with *bdg* in other contexts.

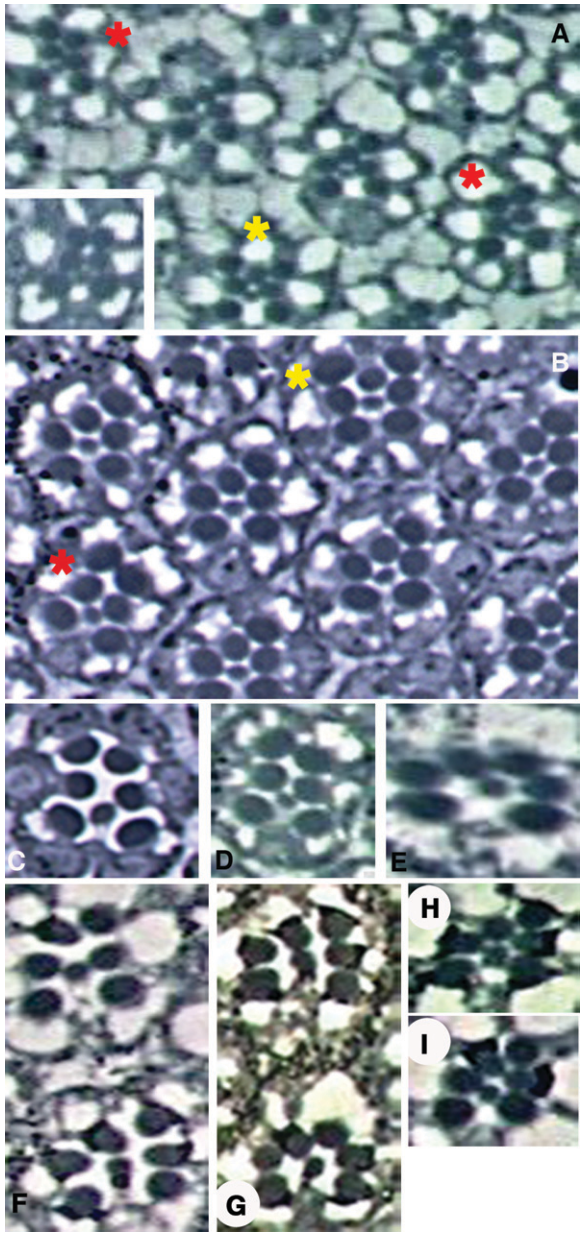

FIGURE 6.—*bdg* mutant phenotype. *bdg* mutant ommatidia are generally phenotypically wild type, although rare ommatidia are missing photoreceptors (not shown), have one extra photoreceptor opposite the R3 cell (yellow asterisks, A and B), are of the R3/R3-type symmetric ommatidia (red asterisks, A and B; inset in A; C and D), or are of the R4/R4-type symmetric ommatidia (E). These phenotypes are evident in a hypomorphic allele, bdg^{164} (A) as well as a null allele, bdg^{90} (B–E). Ommatidia mosaic for the R3/R4 pair are either R3/R3-type (F; $R3^-/R4^+$) or R4/R4-type ($R3^-/R4^+$) ommatidia (G; note that in F and G, one wild-type ommatidium is included to illustrate anterior and posterior), or these mosaic ommatidia are phenotypically wild type (H and I). Phenotypically wild-type mosaic ommatidia can be either $R3^+/R4^-$ (H) or $R3^-/R4^+$ (I). Anterior is to the right.

Loss-of-function *bdg* also displays genetic interactions with loss-of-function alleles of the tissue polarity genes. bdg^{164} dominantly enhances dsh^1, and this interaction can be attributed entirely to a specific enhancement of R3/R3- and R4/R4-type defects (Figure 8, A, B, and E; Table 1). Interestingly, bdg^{164} dominantly suppresses dgo^{380}. Again, as with previously discussed *bdg*/*dgo* interactions, the most significant suppression occurred in the symmetric class of defects (Figure 8, C–E; Table 1).

bdg acts synergistically with all of the core tissue polarity genes (Figure 9). Double homozygous combinations of bdg^{164} and mutations in the core tissue polarity genes *stbm*, *dsh*, *pk*, *fmi*, and *fz* result in a highly statistically significant ($P < 10^{-9}$) enhancement of the homozygous tissue polarity phenotype in all cases (Table 2); homozygosity for both bdg^{164} and dgo^{380} is lethal. The striking enhancement of the $stbm^{6cn}/stbm^{6cn}$, dsh^1/Y, fmi^{frz3}/fmi^{frz3}, and fz^{N21}/fz^{J22} phenotypes by bdg^{164} homozygosity is due almost entirely to the specific increase of both symmetric R3/R3- and R4/R4-type defects (Figure 9, A–D, G, J, and K, respectively; Table 1). The highly statistically significant modification of the pk^{sple}/pk^{sple} phenotype by bdg^{164} homozygosity is unique: while the R3/R3- and R4/R4-type defects are significantly enhanced, D/V inversions are strongly suppressed, resulting in only a modest change in the total percentage of ommatidia with polarity errors (Figure 9, E, F, and K; Table 1).

Bdg influences the regulation of the R3/R4 fates through the tissue polarity complex: The $bdg^{G.MREP}$ overexpression phenotype suggests that *bdg* may influence the R3/R4 cell fates. To determine if *bdg* is required to specify either the R3 or R4 fate, we performed a mosaic analysis of bdg^{90} (a null allele) mutant clones. *bdg* null clones, generated using *ey*-FLP, were notably smaller than standard *ey* clones, typically encompassing as few as several cells up to 10–20 ommatidia (one virtually phenotypically wild-type outlier included ~50 ommatidia). The small size of *bdg* clones is consistent with the small imaginal discs described for bdg^{90} larval escapers.

Two mutant phenotypes occur in ommatidia mosaic for bdg^{90}. First, numerous ommatidia on clonal borders are missing photoreceptors (data not shown). These ommatidia are evidently of mosaic descent, as the remaining photoreceptors in these ommatidia can be either genetically mutant or genetically wild type. Although the genotype of the missing receptors cannot be determined, they are likely to be bdg^- since ommatidia with missing photoreceptors are characteristic of the *bdg* phenotype.

Second, symmetric mosaic ommatidia also occur, although they are relatively rare (Figure 6). Each mosaic symmetric ommatidium identified was mosaic for *bdg* in those cells occupying the R3 and R4 positions, so symmetric ommatidia do not arise unless an ommatidium is mosaic for the R3/R4 pair. Notably, the absence of *bdg* in the remaining photoreceptors (R1, R2, and R5–R8) did not affect the R3/R4 fate decision. The majority of symmetric mosaic ommatidia identified were of the R4/R4 type (Figure 6G), although R3/R3 ommatidia were also found (Figure 6F). In these ommatidia, the cell on the anterior side (*i.e.*, the R3

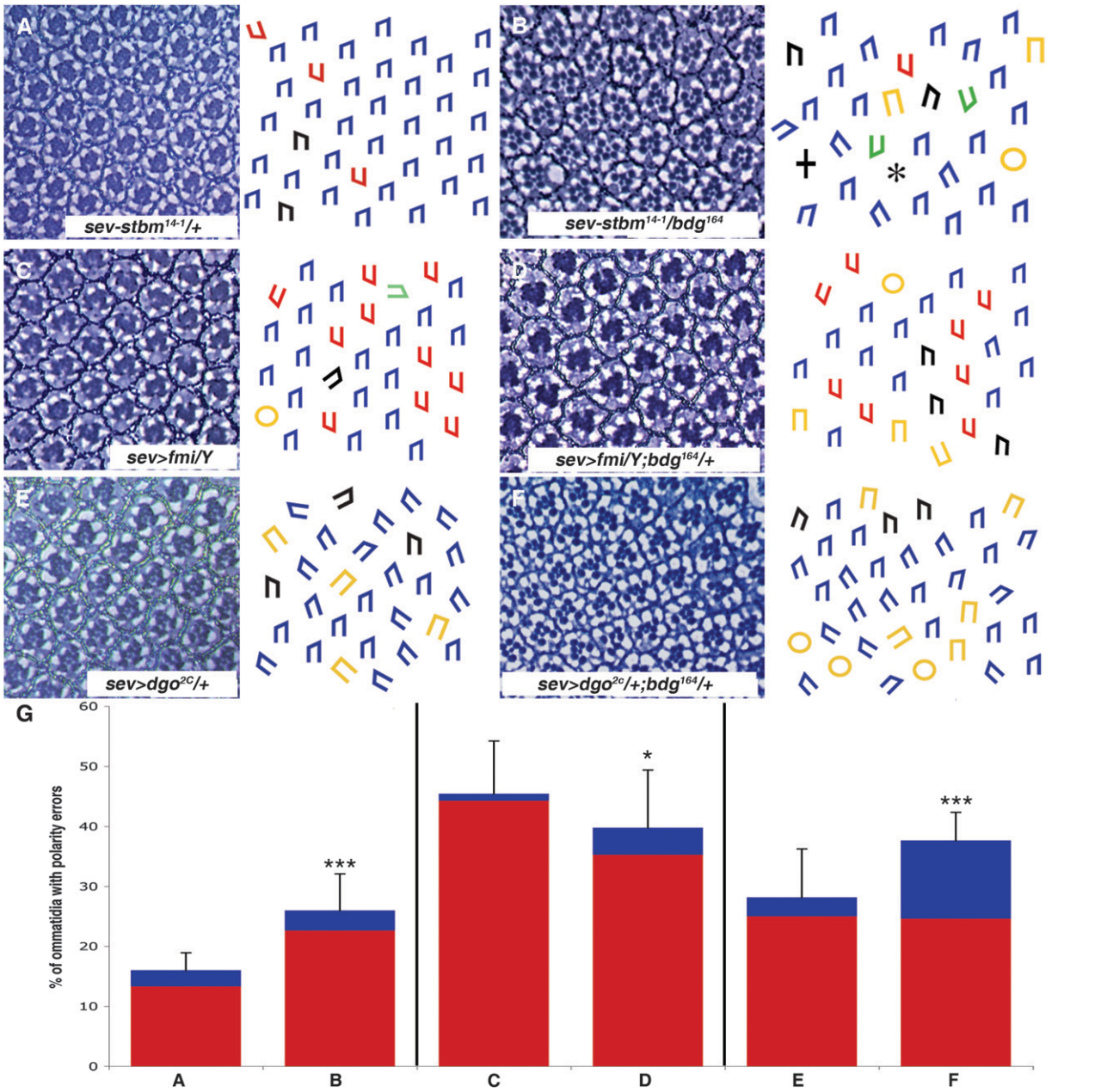

FIGURE 7.—Reduced *bdg* function enhances *sev*-driven tissue polarity phenotypes. Sections of adult eyes (left) and corresponding schematics (right) are shown. bdg^{164}, a hypomorphic allele, enhances the phenotypes of *sev-stbm* (A and B), *sev>fmi* (C and D), and *sev>dgo* (E and F). These genetic interactions are quantified in G (see Table 1 for phenotypic details). Each bar represents the total number of polarity defects; blue represents that portion that are R3/R4 errors and all other classes are depicted as red. Error bars represent SD; single and triple asterisks indicate $P < 10^{-3}$ and 10^{-9}, respectively. Colored trapezoids: blue, wild type; red, D/V inversions; black, A/P inversions; green, AP/DV inversions; yellow rectangles, R3/R3; yellow circles, R4/R4; +, extra cell; *, missing cell. Anterior is to the right.

side) was always mutant whereas the cell on the posterior was always wild type. These observations (i) suggest that *bdg* activity is necessary, but not sufficient, to promote the R3 fate and (ii) raise the possibility that the relative levels of *bdg* activity in R3 and R4 can tip the overall balance in the feedback loop(s) that operate among the tissue polarity proteins in these two cells.

The vast majority of mosaic ommatidia are phenotypically wild type, as is the case with ommatidia composed entirely of photoreceptors that are null for *bdg*. Analysis of mosaic, phenotypically wild-type ommatidia indicates that they can be of the $R3^+/R4^-$ (Figure 6H) or $R3^-/R4^+$ (Figure 6I) genotypes, although more were of the $R3^-/R4^+$genotype.

We also generated bdg^{GMREP} overexpression clones and found that the photoreceptor that overexpressed *bdg* was modestly biased toward the R4 cell fate: in 65% of R3/R4 pairs mosaic for bdg^{GMREP}, the bdg^{GMREP} cell adopted

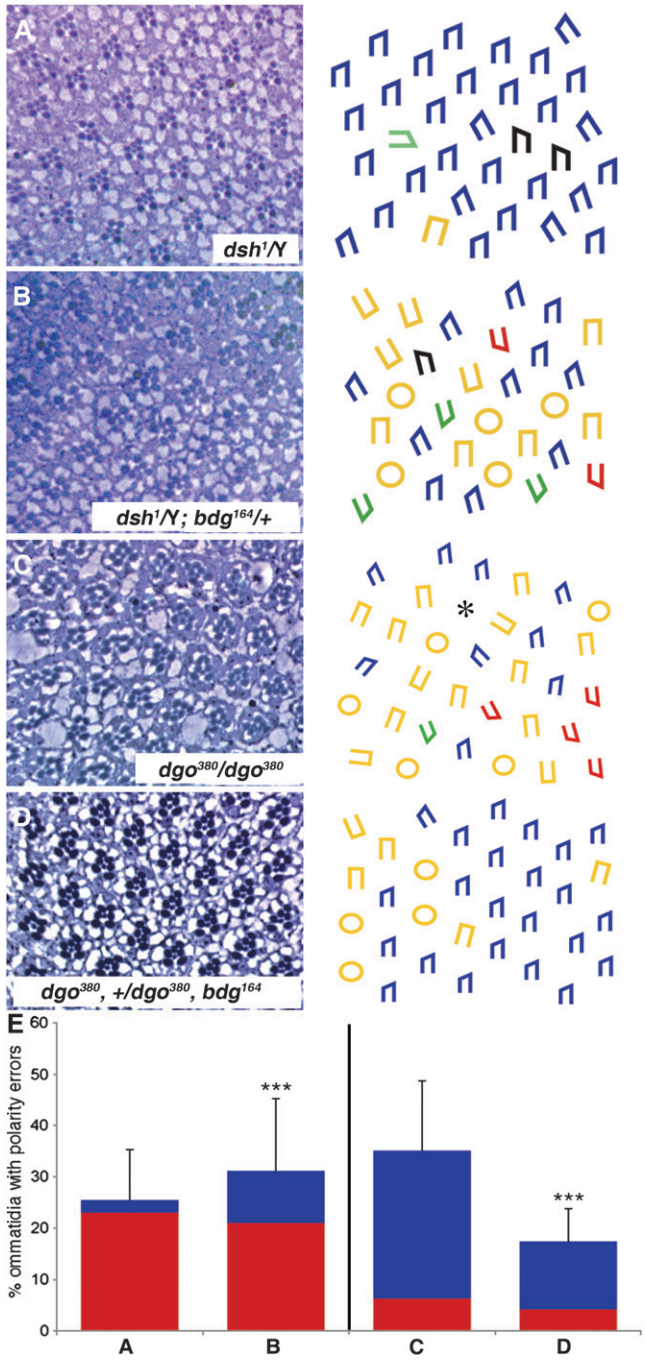

FIGURE 8.—*bdg* dominantly modifies the *dsh* and *dgo* phenotypes. Tangential sections through adult eyes (left) and corresponding schematics (right) are shown. bdg^{164} dominantly enhances dsh^{1} (A and B) and dominantly suppresses dgo^{380} (C and D). These genetic interactions were quantified, as illustrated in E. (See Table 1 for phenotypic details.) Each bar represents the total number of polarity defects; blue represents that portion that are R3/R4 errors and all other classes are depicted as red. Error bars represent SD; triple asterisks indicate $P < 10^{-9}$. Colored trapezoids: blue, wild type; red, D/V inversions; black, A/P inversions; green, AP/DV inversions; yellow rectangles, R3/R3; yellow circles, R4/R4; +, extra cell; *, missing cell. Anterior is to the right.

the R4 fate (data not shown). The consequence of this bias is not clear, as all of these ommatidia are phenotypically wild type. Taken together, the loss-of-function and overexpression mosaic analyses described here do not enable us to make a clear distinction between a potential requirement for *bdg* in either R3 or R4. Rather, they suggest that *bdg* is important generally for the R3/R4 fate decision. In addition, the missing photoreceptor phenotype indicates that *bdg* is necessary but not sufficient for cell viability or recruitment.

***bdg*^{GMREP} is dominantly rescued by all core tissue polarity genes except *fz*:** Haploinsufficiency of *stbm* rescues the bdg^{GMREP} homozygous phenotype from one in which 20.1% of ommatidia have developmental defects to one in which only 3.1% have errors (Table 2). These data suggest that *bdg* may act upstream of *stbm* since reduction in the dose of a downstream signaling molecule can rescue an overexpression phenotype. Interactions between bdg^{GMREP} and the tissue polarity genes were quantitated to define the position of *bdg* in the signaling pathway. Loss-of-function alleles of *dsh*, *pk*, *fmi*, and *dgo*, but not *fz*, also dominantly suppress the homozygous bdg^{GMREP} phenotype (Table 2). Although reduction in an upstream gene can sometimes rescue an overexpression phenotype, here we argue that loss of a downstream gene is the most common mechanism for the suppression of an overexpression phenotype. Under this assumption, these data are consistent with a model in which *bdg* acts upstream of (or in parallel to) *stbm*, *dsh*, *pk*, *fmi*, and *dgo*, but downstream or independently of *fz*.

DISCUSSION

Bdg is a novel regulator of ommatidial polarity that plays a nonessential but integral role in ommatidial polarity by regulating the activity of the tissue polarity complex to influence the R3/R4 cell fates. *bdg* is a unique component of the tissue polarity signaling pathway, as it is the first gene to show selectivity in its interactions with members of the core tissue polarity complex; it acts upstream of, or in parallel to, and yet redundantly with, the core tissue polarity complex to direct the establishment of ommatidial polarity; and it is the first reported suppressor of a loss-of-function tissue polarity phenotype (the symmetrical defects in *dgo*, as described). Furthermore, the nature of the molecule—a predicted transporter—provides an unexpected twist to the current model of how tissue polarity is regulated and suggests a need to think more broadly about the mechanisms that drive this process. In addition to its unique role in regulating polarity, *bdg* plays more global roles as well, as it is also required for viability and the early development of imaginal discs.

Bdg plays a critical and novel role in influencing the R3 and R4 cell fates: *bdg* represents a novel regulator of the R3/R4 fate decision, and the evidence for this role

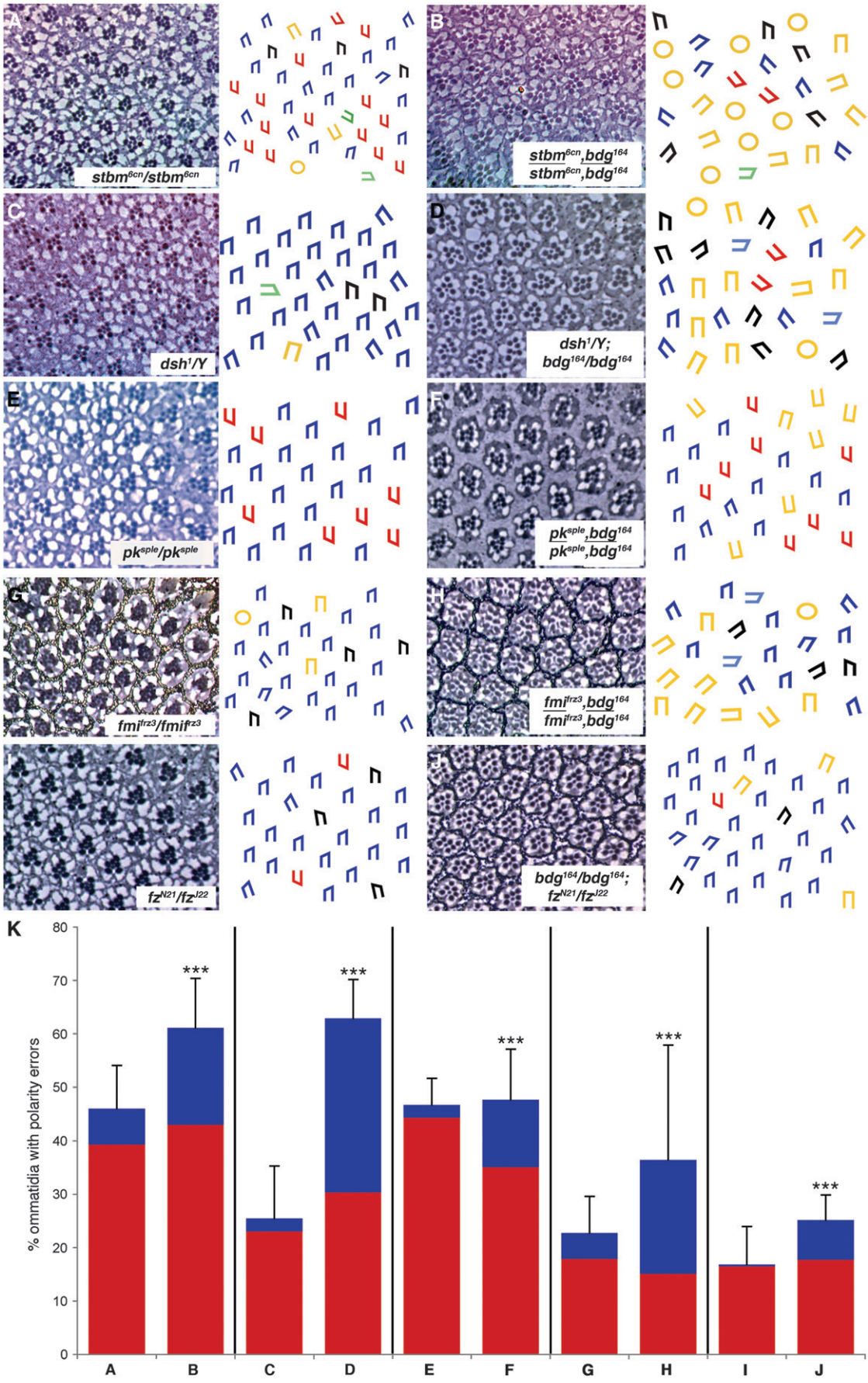
A
stbm6cn/stbm6cn
B
stbm6cn,bdg164
stbm6cn,bdg164
C
dsh1/Y
D
dsh1/Y;
bdg164/bdg164
E
pksple/pksple
F
pksple,bdg164
pksple,bdg164
G
fmifrz3/fmifrz3
H
fmifrz3,bdg164
fmifrz3,bdg164
I
fzN21/fzJ22
J
bdg164/bdg164;
fzN21/fzJ22
K
% ommatidia with polarity errors
0
10
20
30
40
50
60
70
80
***
A
B
C
D
E
F
G
H
I
J

is compelling. First, loss of *bdg* function in tissue polarity mutant backgrounds robustly enhances or suppresses the number of symmetric ommatidia; all other subclasses of polarity defects (for example, AP/DV) are affected to a significantly smaller degree. This specificity suggests that *bdg* acts during the R3/R4 cell fate decision, perhaps at the level of feedback between the presumptive R3 and R4 cells, to ensure that just one cell of each fate is specified in each ommatidium. Second, symmetric ommatidia can arise when *bdg* expression either is reduced or exceeds wild-type levels. While this phenotype reveals a role for *bdg* in the specification of the R3 and R4 cells, it appears to be a redundant role, given the small number of phenotypically mutant ommatidia in *bdg* null clones. However, this role is clearly not insignificant, as indicated by the critical role revealed for *bdg* in the sensitized background of the tissue polarity mutants. Third, symmetric mosaic ommatidia occur only when the R3/R4 pair of cells is mosaic for *bdg*. *bdg* occupies a novel position in the specification of the R3 and R4 cell fates in that it interacts with the tissue polarity genes but perhaps not with the downstream effector and ultimate determinant of the R3/R4 fate decision, Notch.

Furthermore, Bdg is partially redundant with the tissue polarity complex in specifying a single R3 and R4 cell, as mutations in *bdg* synergistically enhance the symmetric errors of all the core tissue polarity genes (with the notable exception of *dgo*). The observation that loss-of-function *bdg* can strongly influence this fate choice in both *fz* and *stbm* mutant backgrounds, gene products for which there is a requirement in R3 and R4, respectively (Zheng *et al.* 1995; Wolff and Rubin 1998), suggests that Bdg function affects the output of the complex at the level of the R3/R4 fates.

***bdg* acts uniquely in the context of *dgo*:** *dgo* is the most recently identified, and least understood, core tissue polarity gene. As such, the cellular function of Dgo has not been fully elucidated. It has been proposed that Dgo is enriched on the R3 side of the R3/R4 border and acts to anchor the polarity proteins to the membrane, a role that is redundant with Pk and Stbm (Mihaly *et al.* 2005).The loss-of-function interaction between *bdg* and *dgo* is unique in that it is the only tissue polarity gene in which the number of symmetric errors is dominantly suppressed by loss-of-function *bdg*, as this class of error is enhanced in *fz*, *dsh*, *stbm*, *pk*, and *fmi*. Similarly, *dgo* is the only tissue polarity gene that is suppressed by bdg^{GMREP}.

Dgo's remarkably distinct response to Bdg function reveals that Dgo is somehow functionally distinct from other members of the complex. Indeed, of all the tissue polarity mutants, *dgo* mutants exhibit, by far, the most penetrant R3/R4 phenotype: ~30% of ommatidia are symmetric (Das *et al.* 2004). This phenotype is particularly interesting in light of the unique interaction between *dgo* and *bdg*, in which *bdg* selectively suppresses the R3/R3- and R4/R4-type ommatidia in *dgo*. The *bdg*/*dgo* interaction could also have a basis in the cellular requirements for, or physical associations between, *bdg* and *dgo*. For example, *bdg* may be localized to either the R3 or the R4 cell, but its cargo required in the other cell. In this case, *bdg* and *dgo* could physically associate in the R3 cell, but *bdg* could be required in both the R3 cell (localization) and the R4 cell (cargo). It is also interesting to note that, in contrast to all other *tissue polarity, bdg* double mutants, *dgo, bdg* homozygotes are lethal. The significance of this interaction is unclear, but would indicate that *dgo* acts with *bdg* in additional developmental contexts.

Neurotransmitter transport may be broadly required during development: The role of neurotransmitter transport in the establishment and maintenance of neuromuscular junction biology is well established; however, only a handful of studies implicate the role of neurotransmission in developmental events. For example, acetylcholine transport is important for the morphology and establishment of neuronal connections during development (Maruyama *et al.* 2001). A role for GABA in Drosophila morphogenesis has also been established—pharmaceutical antagonism of, and RNA interference directed against, the GABA (β(1)) subunit results in reduced hatching, lethality, runting, and trachaeal folding (Dzitoyeva *et al.* 2005). Our identification of a novel role for a putative neurotransmitter transporter in additional developmental processes indicates that roles for neurotransmission may be more diverse than previously recognized.

bdg is predicted to encode a neurotransmitter transporter and belongs to a family of transporters that use the energy generated by the cotransport of Na^+ and Cl^- to move neurotransmitter molecules against a concentration gradient. This protein family shares a common 12-transmembrane helix motif, as well as a

Figure 9.—*bdg* acts synergistically with the core tissue polarity pathway. Sections of adult eyes (left) and corresponding schematics (right) are shown. Double-mutant analysis reveals that bdg^{164} homozygosity enhances the R3/R4 phenotypes of $stbm^{6cn}$ (A and B), dsh^{1} (C and D), pk^{sple} (E and F), fmi^{fz3} (G and H), and fz^{N21}/fz^{J22} (I and J). Notably, the double-mutant combination of $bdg^{164}$and dgo^{380} is lethal. Quantification of these genetic interactions is shown in K. (See Table 1 for phenotypic details.) Each bar represents the total number of polarity defects; blue represents that portion that are R3/R4 errors and all other classes are depicted as red. Error bars represent SD; triple asterisks indicate $P < 10^{-9}$. Colored trapezoids: blue, wild type; red, D/V inversions; black, A/P inversions; green, AP/DV inversions; yellow rectangles, R3/R3; yellow circles, R4/R4; +, extra cell; *, missing cell. Anterior is to the right.

*s*odium:*n*eurotransmitter symporter *f*amily (SNF) domain. The Na^+/Cl^- neurotransmitter transporters can be further divided into four subfamilies on the basis of sequence homology: transporters for GABA, monoamines, the amino acids proline and glycine, and a group of orphan transporters (Lill and Nelson 1998). Our phylogenetic analysis supports the prediction that *bdg* encodes a neurotransmitter transporter and also indicates that Bdg is closely related to the GABA transporter family. While the Bdg cargo has not yet been experimentally defined, we have shown that Bdg does not appear to transport GABA during eye development.

While Bdg's cargo may not be a neurotransmitter, at the very least we can conclude that its cargo is small, as neurotransmitters are only ~100–200 Da. Possible cargoes that fall within these size restrictions include single amino acids (110 Da, on average), ions, and neurotransmitters, but not proteins (for example, Wg is >50 kDa). It is also formally possible that Bdg shares homology with transporters yet functions primarily as a signaling molecule. This is the case with the Drosophila protein Pathetic, which, although annotated as an amino acid transporter, regulates growth via a nutrient-sensing mechanism that functions independently of bulk amino acid transport (Goberdhan *et al.* 2005).

Bedraggled—transporter of elusive factor X? A long-standing model for ommatidial polarity invokes the activity of a long-range morphogen that establishes a gradient of polarizing activity across the developing eye (Wehrli and Tomlinson 1998). In spite of extensive efforts dedicated to the identification of this predicted morphogen, termed Factor X, it has not yet been uncovered. It has long been assumed that the morphogen is a protein. However, if the morphogen is instead a small molecule, it would have been missed in genetic screens since its identity would have precluded it from the pool of candidates. The discovery of Bdg, the only transporter protein implicated in ommatidial polarity to date, points to a possible role for Bdg as a transporter of a non-Wnt morphogen, provided Bdg acts independently of *fz* (our genetic analysis does indicate that *bdg* acts downstream or independently of *fz*). Several observations support the validity of this possibility. First, Bdg makes a critical contribution to the R3/R4 fate decision, which is thought to be a functional readout of Factor X, indicating that the transport of some small molecule plays a role in this fate decision. Second, *bdg* transcript is enriched at the wings of the third instar eye imaginal disc, a pattern that has been predicted for a factor that acts in long-range signaling in the eye (Wehrli and Tomlinson 1998). Third, Bdg has been predicted to symport an unknown neurotransmitter along with sodium, a cation (BDGP annotation). Intriguingly, cations are among a handful of small molecules that have established roles in long-range activity in some developmental contexts, for example, the role of calcium in setting up the D/V axis in embryos (Creton *et al.* 2000) and the essential role of the H^+/K^+-ATPase transporter in orienting the left–right body axis in Xenopus (Levin *et al.* 2002).

While this global transport hypothesis is within the realm of possibility, we favor a model in which Bdg contributes to the establishment of ommatidial polarity by facilitating local (*i.e.*, between R3 and R4), rather than global, transport. More specifically, Bdg may transport a signal between members of the tissue polarity complex to modulate R3/R4 cell fate specification. Such a locally transported signal could have global results if it is perpetuated via cell–cell relay across the eye primordium. This revised hypothesis would indicate that Bdg represents a reasonable candidate for the transporter of "Factor X." The identification of the Bdg cargo will be necessary to test this potential mechanism.

We thank B. Hay for generously providing the Glass Multimer Reporter Enhancer-Promoter (GMREP) collection; J. Glasscock for analyzing the *bdg* intronic region; J. First for technical assistance; S. Dutcher for assistance with the phylogenetic analysis; B. Hay, D. Strutt, D. Gubb, M. Mlodzik, T. Uemura, and the Bloomington Stock Center for providing fly stocks; B. Hay and T. Uemura for providing antibodies; B. Hay, D. Wassarman, and H. Chang for scientific guidance; and D. Strutt, H. Chang, and A. DiAntonio for critical comments on the manuscript. This work was supported by a Lucille P. Markey Pathway fellowship to A.S.R. and by National Institutes of Health grant R01 EY13136 to T.W.

LITERATURE CITED

Altschul, S. F., and D. J. Lipman, 1990 Protein database searches for multiple alignments. Proc. Natl. Acad. Sci. USA **87:** 5509–5513.

Arredondo, L., H. B. Nelson, K. Beckingham and M. Stern, 1998 Increased transmitter release and aberrant synapse morphology in a Drosophila *Calmodulin* mutant. Genetics **150:** 265–274.

Beall, E. L., M. B. Mahoney and D. C. Rio, 2002 Identification and analysis of a hyperactive mutant form of Drosophila *P*-element transposase. Genetics **162:** 217–227.

Chae, J., M. J. Kim, J. H. Goo, S. Collier, D. Gubb *et al.*, 1999 The Drosophila tissue polarity gene starry night encodes a member of the protocadherin family. Development **126:** 5421–5429.

Cooper, M. T., and S. J. Bray, 1999 Frizzled regulation of Notch signalling polarizes cell fate in the Drosophila eye. Nature **397:** 526–530.

Creton, R., J. A. Kreiling and L. F. Jaffe, 2000 Presence and roles of calcium gradients along the dorsal-ventral axis in Drosophila embryos. Dev. Biol. **217:** 375–385.

Dabdoub, A., M. J. Donohue, A. Brennan, V. Wolf, M. Montcouquiol *et al.*, 2003 Wnt signaling mediates reorientation of outer hair cell stereociliary bundles in the mammalian cochlea. Development **130:** 2375–2384.

Das, G., A. Jenny, T. J. Klein, S. Eaton and M. Mlodzik, 2004 Diego interacts with Prickle and Strabismus/Van Gogh to localize planar cell polarity complexes. Development **131:** 4467–4476.

Dzitoyeva, S., A. Gutnov, M. Imbesi, N. Dimitrijevic and H. Manev, 2005 Developmental role of GABAB(1) receptors in Drosophila. Brain Res. Dev. Brain Res. **158:** 111–114.

Fanto, M., C. A. Mayes and M. Mlodzik, 1998 Linking cell-fate specification to planar polarity: determination of the R3/R4 photoreceptors is a prerequisite for the interpretation of the Frizzled mediated polarity signal. Mech. Dev. **74:** 51–58.

Feiguin, F., M. Hannus, M. Mlodzik and S. Eaton, 2001 The ankyrin repeat protein Diego mediates Frizzled-dependent planar polarization. Dev. Cell **1:** 93–101.

Goberdhan, D. C., D. Meredith, C. A. Boyd and C. Wilson, 2005 PAT-related amino acid transporters regulate growth via a novel mechanism that does not require bulk transport of amino acids. Development **132:** 2365–2375.

Godenschwege, T. A., D. Reisch, S. Diegelmann, K. Eberle, N. Funk *et al.*, 2004 Flies lacking all synapsins are unexpectedly healthy but are impaired in complex behaviour. Eur. J. Neurosci. **20:** 611–622.

Gubb, D., C. Green, D. Huen, D. Coulson, G. Johnson *et al.*, 1999 The balance between isoforms of the prickle LIM domain protein is critical for planar polarity in Drosophila imaginal discs. Genes Dev. **13:** 2315–2327.

Hay, B. A., R. Maile and G. M. Rubin, 1997 P element insertion-dependent gene activation in the Drosophila eye. Proc. Natl. Acad. Sci. USA **94:** 5195–5200.

Huh, J. R., I. Foe, I. Muro, C. H. Chen, J. H. Seol *et al.*, 2007 The Drosophila inhibitor of apoptosis (IAP) DIAP2 is dispensable for cell survival, required for the innate immune response to gram-negative bacterial infection, and can be negatively regulated by the reaper/hid/grim family of IAP-binding apoptosis inducers. J. Biol. Chem. **282:** 2056–2068.

Kearney, J. B., S. R. Wheeler, P. Estes, B. Parente and S. T. Crews, 2004 Gene expression profiling of the developing Drosophila CNS midline cells. Dev. Biol. **275:** 473–492.

Klingensmith, J., R. Nusse and N. Perrimon, 1994 The Drosophila segment polarity gene dishevelled encodes a novel protein required for response to the wingless signal. Genes Dev. **8:** 118–130.

Leal, S. M., and W. S. Neckameyer, 2002 Pharmacological evidence for GABAergic regulation of specific behaviors in Drosophila melanogaster. J. Neurobiol. **50:** 245–261.

Levin, M., T. Thorlin, K. R. Robinson, T. Nogi and M. Mercola, 2002 Asymmetries in H+/K+-ATPase and cell membrane potentials comprise a very early step in left-right patterning. Cell **111:** 77–89.

Lill, H., and N. Nelson, 1998 Homologies and family relationships among Na+/Cl- neurotransmitter transporters. Methods Enzymol. **296:** 425–436.

Maruyama, H., T. L. Rakow and I. N. Maruyama, 2001 Synaptic exocytosis and nervous system development impaired in Caenorhabditis elegans unc-13 mutants. Neuroscience **104:** 287–297.

Mihaly, J., T. Matusek and C. Pataki, 2005 Diego and friends play again. FEBS J. **272:** 3241–3252.

Mlodzik, V. E. M., 2005 *Planar Cell Polarization During Development*. Elsevier, New York.

Myers, D. C., D. S. Sepich and L. Solnica-Krezel, 2002 Bmp activity gradient regulates convergent extension during zebrafish gastrulation. Dev. Biol. **243:** 81–98.

Nichols, C. D., J. Ronesi, W. Pratt and E. Sanders-Bush, 2002 Hallucinogens and Drosophila: linking serotonin receptor activation to behavior. Neuroscience **115:** 979–984.

Rawls, A. S., and T. Wolff, 2003 Strabismus requires Flamingo and Prickle function to regulate tissue polarity in the Drosophila eye. Development **130:** 1877–1887.

Rawls, A. S., J. B. Guinto and T. Wolff, 2002 The cadherins fat and dachsous regulate dorsal/ventral signaling in the Drosophila eye. Curr. Biol. **12:** 1021–1026.

Rubin, G. M., and A. C. Spradling, 1982 Genetic transformation of Drosophila with transposable element vectors. Science **218:** 348–353.

Sambrook, J., E. F. Fritsch and T. Maniatis, 1989 *Molecular Cloning: A Laboratory Manual*, Ed. 2. Cold Spring Harbor Laboratory Press, Plainview, NY.

Sokal, R., and F. Rohlf, 1995 *Biometry: The Principles and Practice of Statistics in Biological Research*, Ed. 3. W. H. Freeman, San Francisco.

Sonnhammer, E. L., G. von Heijne and A. Krogh, 1998 A hidden Markov model for predicting transmembrane helices in protein sequences. Proc. Int. Conf. Intell. Syst. Mol. Biol. **6:** 175–182.

Strutt, H., J. Mundy, K. Hofstra and D. Strutt, 2004 Cleavage and secretion is not required for four-jointed function in Drosophila patterning. Development **131:** 881–890.

Taylor, J., N. Abramova, J. Charlton and P. N. Adler, 1998 Van Gogh: a new Drosophila tissue polarity gene. Genetics **150:** 199–210.

Theisen, H., J. Purcell, M. Bennett, D. Kansagara, A. Syed *et al.*, 1994 dishevelled is required during wingless signaling to establish both cell polarity and cell identity. Development **120:** 347–360.

Thompson, J. D., T. J. Gibson, F. Plewniak, F. Jeanmougin and D. G. Higgins, 1997 The CLUSTAL_X windows interface: flexible strategies for multiple sequence alignment aided by quality analysis tools. Nucleic Acids Res. **25:** 4876–4882.

Tomlinson, A., and G. Struhl, 1999 Decoding vectorial information from a gradient: sequential roles of the receptors Frizzled and Notch in establishing planar polarity in the Drosophila eye. Development **126:** 5725–5738.

Tree, D. R., J. M. Shulman, R. Rousset, M. P. Scott, D. Gubb *et al.*, 2002 Prickle mediates feedback amplification to generate asymmetric planar cell polarity signaling. Cell **109:** 371–381.

Usui, T., Y. Shima, Y. Shimada, S. Hirano, R. W. Burgess *et al.*, 1999 Flamingo, a seven-pass transmembrane cadherin, regulates planar cell polarity under the control of Frizzled. Cell **98:** 585–595.

Vinson, C. R., and P. N. Adler, 1987 Directional non-cell autonomy and the transmission of polarity information by the frizzled gene of Drosophila. Nature **329:** 549–551.

Vinson, C. R., S. Conover and P. N. Adler, 1989 A Drosophila tissue polarity locus encodes a protein containing seven potential transmembrane domains. Nature **338:** 263–264.

Wehrli, M., and A. Tomlinson, 1998 Independent regulation of anterior/posterior and equatorial/polar polarity in the Drosophila eye; evidence for the involvement of Wnt signaling in the equatorial/polar axis. Development **125:** 1421–1432.

Wolff, T., 2000a Histological techniques for the Drosophila eye. Part I: larva and pupa, pp. 200–227 in *Drosophila Protocols*, edited by W. Sullivan, M. Ashburner and R. S. Hawley. Cold Spring Harbor Laboratory Press, Cold Spring Harbor, NY.

Wolff, T., 2000b Histological techniques for the Drosophila eye. Part II: adult, pp. 228–243 in *Drosophila Protocols*, edited by W. Sullivan, M. Ashburner and R. S. Hawley. Cold Spring Harbor Laboratory Press, Cold Spring Harbor, NY.

Wolff, T., and G. M. Rubin, 1998 Strabismus, a novel gene that regulates tissue polarity and cell fate decisions in Drosophila. Development **125:** 1149–1159.

Wolff, T., J. B. Guinto and A. S. Rawls, 2007 Screen for genetic modifiers of stbm reveals that photoreceptor fate and rotation can be genetically uncoupled in the Drosophila eye. PLoS ONE **2:** e453.

Yang, C. H., J. D. Axelrod and M. A. Simon, 2002 Regulation of Frizzled by fat-like cadherins during planar polarity signaling in the Drosophila compound eye. Cell **108:** 675–688.

Zeidler, M. P., N. Perrimon and D. I. Strutt, 1999 The four-jointed gene is required in the Drosophila eye for ommatidial polarity specification. Curr. Biol. **9:** 1363–1372.

Zheng, L., J. Zhang and R. W. Carthew, 1995 frizzled regulates mirror-symmetric pattern formation in the Drosophila eye. Development **121:** 3045–3055.

Communicating editor: T. R. Magnuson